Cold atmospheric plasma induces apoptosis in human colon and lung cancer cells through modulating mitochondrial pathway

Yanhong Wang[1], Xinyu Mang[2], Xuran Li[1], Zhengyu Cai[3] and Fei Tan[1,4,5]*

[1]Shanghai Fourth People's Hospital, School of Medicine, Tongji University, Shanghai, China, [2]Department of Biochemistry and Molecular Biology, State Key Laboratory of Medical Molecular Biology, Institute of Basic Medical Sciences Chinese Academy of Medical Sciences, School of Basic Medicine Peking Union Medical College, Beijing, China, [3]Tongji University Cancer Center, Shanghai Tenth People's Hospital, School of Medicine, Tongji University, Shanghai, China, [4]The Royal College of Surgeons in Ireland, Dublin, Ireland, [5]The Royal College of Surgeons of England, London, United Kingdom

Cold atmospheric plasma (CAP) is an emerging and promising oncotherapy with considerable potential and advantages that traditional treatment modalities lack. The objective of this study was to investigate the effect and mechanism of plasma-inhibited proliferation and plasma-induced apoptosis on human lung cancer and colon cancer cells *in vitro* and *in vivo*. Piezobrush® PZ2, a handheld CAP unit based on the piezoelectric direct discharge technology, was used to generate and deliver non-thermal plasma. Firstly, CAP_{PZ2} treatment inhibited the proliferation of HT29 colorectal cancer cells and A549 lung cancer cells using CCK8 assay, caused morphological changes at the cellular and subcellular levels using transmission electron microscopy, and suppressed both types of tumor cell migration and invasion using the Transwell migration and Matrigel invasion assay. Secondly, we confirmed plasma-induced apoptosis in the HT29 and A549 cells using the AO/EB staining coupled with flow cytometry, and verified the production of apoptosis-related proteins, such as cytochrome c, PARP, cleaved caspase-3 and caspase-9, Bcl-2 and Bax, using western blotting. Finally, the aforementioned *in vitro* results were tested *in vivo* using cell-derived xenograft mouse models, and the anticancer effect was confirmed and attributed to CAP-mediated apoptosis. The immunohistochemical analysis revealed that the expression of cleaved caspase-9, caspase-3, PARP and Bax were upregulated whereas that of Bcl-2 downregulated after CAP treatment. These findings collectively suggest that the activation of the mitochondrial pathway is involved during CAP_{PZ2}-induced apoptosis of human colon and lung cancer cells *in vitro* and *in vivo*.

KEYWORDS

cold atmospheric plasma, apoptosis, reactive oxygen species, mitochondria, caspase

Introduction

Cancer is a leading cause of death worldwide, accounting for nearly 10 million deaths in 2020 (Ferlay et al., 2021). Colon cancer and lung cancer are among the top three cancers in terms of number of new cases (1.9 and 2.2 million) and number of cancer death (0.9 and 1.8 million), respectively. Depending on the cancer staging, the main treatment options for these prevalent and lethal malignancies include, but are not limited to, surgery, chemotherapy, and radiation therapy. However, the prognosis of colon and lung cancer has never been satisfying, especially for patients with metastatic lesions. As new optional approach, targeted therapy and immunotherapy have successfully prolonged overall survival for these patients, collectively changing the treatment paradigm of colon cancer and lung cancer. Nonetheless, these newer treatment modalities have limitations. Therefore, there is a constant drive to seek more versatile and adaptable oncotherapy.

As a new biomedical technology, cold atmospheric plasma (CAP) is an ionized non-thermal gas mixture composed of various reactive oxygen species (ROS), reactive nitrogen species and ultraviolet photons (Fridman et al., 2008; Ratovitski et al., 2014; von Woedtke et al., 2019). CAP has demonstrated great potential in cancer treatment (Arndt et al., 2013; Adhikari et al., 2019). Since the killing effect of CAP on melanoma was first reported, the research on the application of CAP in oncology has progressed rapidly (Binenbaum et al., 2017). Many studies have shown that CAP can inhibit tumor growth and promote tumor death in various malignant tumor cells, including but are not limited to, hepatocellular carcinoma cells, melanoma cells, prostate cancer cells, cervical cancer cells, cervical squamous cell carcinoma cells, oral squamous cell carcinoma cells, osteosarcoma cells, multiple myeloma cells, lymphoma cells (Walk et al., 2013; Gumbel et al., 2016; Cheng et al., 2017; Yan et al., 2017). CAP can not only selectively induce tumor cell apoptosis, but also inhibit tumor cell migration and invasion (Xu et al., 2017). In addition, CAP enhances the sensitivity of tumor cells to chemotherapeutic drugs (Ishaq et al., 2015), achieving antitumor effect with high efficiency and low toxicity. Meanwhile, some studies have confirmed that the synergistic effect of CAP and nanoparticles renders stronger antineoplastic ability (Aryal and Bisht, 2017). However, the exact mechanism of CAP's oncological advantage is not completely elucidated, and it might be related to its active components, such as ultraviolet, charged particles, and chemically active elements (Volotskova et al., 2012).

CAP is a type of low-temperature plasma, which produces various free radicals that are suitable for medical treatment (Wang et al., 2013). CAP damages cancer cells intracellularly, such as destroying DNA and mitochondria leading to apoptosis of the treated cells (Kim et al., 2010; Ahn et al., 2011). These changes are mainly due to the accumulation of intracellular ROS in cancer cells, resulting in mitochondrial dysfunction, sub-G1 arrest and DNA damage (Lee et al., 2016). Compared to normal cells, cancer cells are more likely to accumulate ROS because of the increased production rate of ROS, which promote several aspects of cancer cell proliferation and metastasis (Liou and Storz, 2010). According to previous studies, the production of ROS may be the main underlying mechanism of CAP-induced apoptosis (Wang et al., 2019).

We were the first to use the newly developed Piezobrush compact handheld plasma device, which is based on the piezoelectric direct discharge (PDD) technology, on cancer treatment. The primary objective of this study was to evaluate the influence of the above plasma platform, CAP_{PZ2}, on human colon and lung cancer cells, highlighting the effect of CAP_{PZ2} treatment on the proliferation, migration/invasion, and apoptosis of HT29 and A549 cells *in vitro* and *in vivo*. The secondary objective was to explore the potential molecular mechanism of plasma-induced apoptosis in the colorectal and pulmonary cancer model. This provides new insights for the clinical treatment of colon cancer and lung cancer, potentially serving as a novel oncotherapy.

Materials and methods

Cell culture

Human colorectal adenocarcinoma HT29 cells and human lung adenocarcinoma A549 cells were kindly provided by Professor Zhenyu Cai (Tongji University, Shanghai, China). These cells were cultured at 37°C with 5% CO_2 in The Piezobrush® PZ2 model was used (Tinsley and Harris, 2020) and has been conceived to be an efficient handheld unit (Figures 1A,B). The CAP_{PZ2} device, at a maximum power consumption of 30 W, generated cold active plasma with an a nozzle temperature of <50°C. The plasma nozzle was placed 10 mm above the treated surface, with treatment duration of 15, 30, 60 and 120 s (Figures 1C,D). In order to examine the effect of CAP_{PZ2} treatment on various tumor cells, we performed a direct plasma treatment on the HT29 and A549 cells without coverage by the cell culture medium. This contrasts with indirect plasma treatment used in some other studies, e.g., plasma-activated medium (PAM).

A complete cell growth medium containing DMEM (Corning, United States), 10% fetal bovine serum (FBS) and 1% penicillin and streptomycin (Gibco, United States). The cells were cultured to a confluence of 85%–90% and then subcultured using 0.25% trypsin (Gibco, United States). The cells were gathered in the exponential growth phase.

Cold atmospheric plasma treatment

The plasma device used in this study is an ambient air-dependent device that was designed and developed by Relyon Plasma GmbH (Regensburg, Germany).
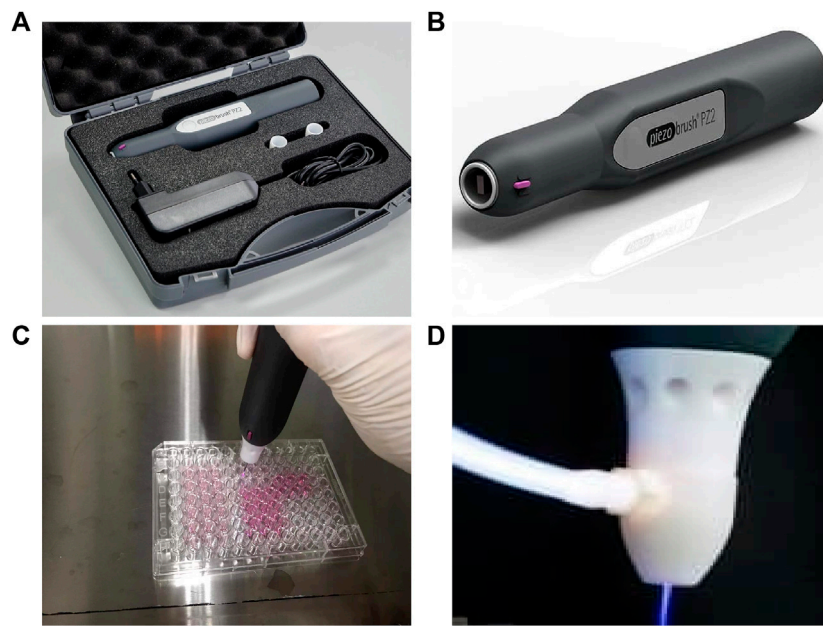
FIGURE 1
Illustration of the CAP device, Piezobrush® PZ2, used in this study. **(A,B)** Content and portability of the CAP_{PZ2} kit. **(C)** Cellular treatment using the handheld plasma device. **(D)** Close-up of the plasma nozzle in the operating mode.

Cell counting kit-8 assay

The inhibitory effect of CAP_{PZ2} on HT29 and A549 cell proliferation was measured using Cell Counting Kit-8 (CCK8, Dojindo Laboratories, Japan) assay. CAP_{PZ2} was attached to a small stereotaxic apparatus with its tip adjusted to a height of 10 mm above the fluid level of cell culture. CAP_{PZ2} was then administered for designated time period. After 24 h of incubation, the cells were treated by CAP_{PZ2} (0, 15, 30, 60 and 120 s) in 96 well-plates (3×10^3 cells/well) and incubated for a further 24 h. Following CAP_{PZ2} treatment, CCK8 assay was performed according to manufacturer's instructions at 37°C for 2 h. The absorbance was read at 450 nm using an ELISA microplate reader (Molecular Devices, Sunnyvale, United States). All experiments were performed in triplicates.

Hoechst fluorescent staining

The HT29 and A549 cells were seeded in 12-well plates and exposed to CAP_{PZ2} treatment for 15, 30 and 60 sec. Following incubation of 24 h, the cells were stained with Hoechst 33342 (Beyotime Biotechnology, China) at 37°C for 30 min, and then washed twice with phosphate-buffered saline (PBS) for three

minutes each. Nuclear morphological changes were observed using an Olympus fluorescent microscopy.

Transmission electron microscopy

The HT29 and A549 cells were treated with CAP_{PZ2} (30 s) at 37°C for 24 h and then collected for electron microscopy. Firstly, the cell precipitates were fixed in 5% glutaraldehyde for 30 min, and then placed in 1% osmium tetroxide and 0.1 mol/L sodium cacodylate (pH 7.4) for 1 h. The cell precipitates were desiccated in a graded series of acetone and embedded with EPON-812. Ultra-thin sections were prepared, double-stained with uranium and plumbum, and observed under transmission electron microscope using x10,000 magnification. Meanwhile, untreated cells were used as control.

Transwell migration and invasion assay

Cell motility and invasiveness were measured using the Transwell assay (Millipore, Billerica, United States). The HT29 and A549 cells were seeded into 6-well plates at a density of 2×10^5 cells/well and treated with the CAP_{PZ2} (0, 30 and 60 s, respectively). For the migration assay, approximately

200 μL of 1×10^5 HT29 or A549 cells were seeded into the upper chamber containing serum-free medium, while the bottom of the chamber contained 800 μL of DMEM with 10% FBS. For the invasion assay, the chamber was coated with 100 μL of Matrigel (BD Biosciences, United States), and the subsequent steps were similar to those of the migration assay. After 24–48 h of incubation, the medium was discarded. Cells that had invaded the lower surface of the membrane were fixed in Methanol for 30 min and stained with 0.1% crystal violet for 30 min. Migrated and invaded cells in random fields were examined and counted using Olympus microscopy at ×200 magnification.

RNA extraction and qRT-PCR

Four metastasis-associated messenger RNA (mRNA) gene expression (*MMP9*, *MMP2*, *VEGF*, *MTDH*) was detected regarding different times of CAP_{PZ2} treatment. Briefly, HT29 and A549 cells were seeded in 6-well plate and incubated 24 h. CAP_{PZ2} treatment homogeneity was then conducted with 30 and 60 s and cells were allowed growth for another 24 h. Total RNA was extracted from cell using Trizol reagent (Invitrogen) according to the manufacturer's instruction. The NanoDrop1000 Spectrophotometer (ThermoScientific) was employed to quantify the amount of RNA samples. Specifically, 1 μg of total RNA was utilized for reverse transcription using RevertAid First Strand cDNA Synthesis kit (Thermo Fisher Scientific). The qRT-PCR was performed using the ABI 7500 Real-Time PCR System (Applied Biosystems) to verify gene expression in various cells. qRT-PCR was performed using PowerUp SYBR Green Master Mix (Applied Biosystems). The primer sequences are forMMP9: forward, 5′-AGACCTGGG CAGATTCCAAAC-3′ and reverse, 5′-CGGCAAGTCTTCCGA GTAGT-3′; for MMP2: forward, 5′-GATACCCCTTTGACG GTAAGGA-3′ and reverse, 5′-CCTTCTCCCAAGGTCCAT AGC-3′; for VEGF: forward, 5′-AGGGCAGAATCATCACGA AGT-3′ and reverse, 5′-AGGGTCTCGATTGGATGGCA-3′; for MTDH: forward, 5′-AAGCAGTGCAAAACAGTTCACG-3′ and reverse, 5′-GCACCTTATCACGTTTACGCT-3′. The cells without CAP_{PZ2} treatment were selected as control.

Detection of apoptosis

The HT29 and A549 cells were seeded into 6-well plates at a density of 2×10^5 cells/well and exposed to CAP_{PZ2} treatment for 30 and 60 s. After treatment for 24 h, the cells were detached and stained using PE Annexin V apoptosis detection kit I (BD Biosciences, San Jose, CA, United States), according to manufacturer's instructions. In brief, the HT29 or A549 cells were collected after CAP_{PZ2} treatment, washed with cold PBS and incubated at room temperature with PE Annexin V and 7-AAD for 15 min in darkness. Flow cytometry analysis was performed

within 1 h. The HT29 or A549 cells were separated using the BD LSRFortessa™ flow cytometer (BD Biosciences). At least 20,000 cells were analyzed from each treatment group.

Acridine orange and ethidium bromide cell staining

The acridine orange and ethidium bromide (AO/EB) (BestBio, China) staining was used to distinguish viable cells from apoptotic and necrotic cells. The HT29 and A549 cells (1×10^5 cells/well) were inoculated in 24-well plates and allowed to adhere for 12 h. These cells were then treated using CAP_{PZ2} (30 and 60 s) for 24 h. The HT29 and A549 cells were harvested, centrifuged, resuspended in 100 μl of culture medium, and stained with 5 μl AO and EB, respectively. The cell suspension was immediately examined using fluorescence microscopy (Olympus), and the obtained images were analyzed accordingly. Cells with uniformly bright green nuclei and an organized structure were considered as viable cells, those with orange to red nuclei, condensed to fragmented chromatin and green cytoplasm as apoptotic cells, and those with uniformly orange to red nuclei, an organized structure and red cytoplasm as necrotic cells.

Measurement of reactive oxygen species

The HT29 and A549 cells were seeded in 6-well culture plates at a density of 2×10^5 cells/well and treated using CAP_{PZ2} at 0, 30 and 60 s for 24 h. The cells were harvested, washed, and resuspended in serum-free DMEM. The resuspended cells were stained with 10 μM fluorescent dye DCFH-DA (Beyotime Biotechnology, China) at 37°C for 20 min, and rewashed 3 times by PBS. The fluorescence from the HT29 and A549 cells were measured using the BD LSRFortessa™ flow cytometer (BD Biosciences). At least 10,000 cells were analyzed from each treatment group.

Western blot

The HT29 and A549 cells were cultured in 6-well plates at a density of 2×10^5 cells/well and treated using CAP_{PZ2} (0, 30 and 60 s, respectively). After 24 h, cells were harvested and washed with PBS solution. The whole-cell lysates were prepared using RIPA lysis buffer (Solaibao, Beijing, China) containing cOmplete™ Protease Inhibitor Cocktail tablets (Roche, Indianapolis, IN). Protein concentrations were quantified using a BCA protein assay kit (Solaibao, Beijing, China) according to the instructions. For the western blotting analysis, 40 μg of protein from each sample was loaded into 10%–15% SDS-PAGE and transferred onto a PVDF membrane

(Immobilon-P, CA, United States). The membranes were incubated overnight at 4°C with suitably diluted primary antibodies against cytochrome c, cleaved poly (ADP-ribose) polymerase (cleaved-PARP), cleaved caspase-3, cleaved caspase-9, Bcl-2 or Bax (Cell Signaling Technology, United States). The signals were developed using an enhanced chemiluminescence (ECL) kit (Immobilon-P, CA, United States), and the bands visualized using the ChemiDoc™ Touch Image system (Bio-Rad).

Nude mice xenograft model

Thirty-two female BALB/c nude mice were purchased from Zhejiang Vital River Laboratory Animal Technology Co., Ltd. (Zhejiang, China, SCXK (ZHE) 2019-0001, Animal Certificate No.: 20211111Abzz0619000810), and housed under controlled temperature (22–24°C) and pathogen-free conditions at the Experimental Animal Center, School of Medicine, Tongji University. All procedures were performed aseptically in accordance with the standard guidelines under a protocol approved by the Experimental Animal Ethics Committee of Tongji University. The HT29 or A549 cells (5×10^6 cells) were inoculated subcutaneously into the right anterior armpit of nude mice when the mice turned 6 weeks old. When the tumor size reached approximately 50 mm³, these mice were randomly divided into control and CAP_{PZ2} groups ($n = 8$ each). The animals in the CAP_{PZ2} group were treated for 2 min each time and thrice weekly until the end of the study. The tumor volume (V) was determined by measuring the length (a) and width (b) every 3 or 4 days and calculated using the following formula: V (mm³) = ½ x ab². All mice were sacrificed, and tumors were collected and weighed 24 h after the last treatment.

Histology and immunostaining

Mouse tumours were resected, fixed in 10% neutral buffered formalin overnight at 4°C, and paraffin embedded. Five-micrometre sections were processed for hematoxylin and eosin (HE) or mmunohistochemical (IHC) staining per standard protocol. For immunohistochemistry staining, tissue sections were first deparaffinized in xylene and rehydrated in graded ethanols. Then, the tumor slides were immersed in methanol containing 0.1% hydrogen peroxide for 10 min to block endogenous peroxidase activity. Antigen repair was performed by treating the slides with pH 6.0 citrate buffer for 20 min in a microwave oven. The cytochrome c (Cell Signaling Technology, 1:100), cleaved PARP (Cell Signaling Technology, 1:100), cleaved caspase-3 (Cell Signaling Technology, 1:100), Bcl-2 (Cell Signaling Technology, 1:100), Bax (Cell Signaling Technology, 1:200) and ki67 (Abcam, 1:200) primary antibodies were used for immunohistochemistry according to

a standard avidin-biotin complex (ABC) method. The sections were then incubated with appropriate biotinylated secondary antibodies provided in the ABC kit (PV-6000D, Beijing Zhongshan Jinqiao Biotechnology Co., Ltd) and visualized by exposure to diaminobenzidine substrate. The sections were finally counterstained with hematoxylin before dehydration, removal and sealing.

Statistical analysis

All statistical calculations were performed using the GraphPad Prism 7 software package (GraphPad Software Inc., United States). Results were expressed as mean ± SD. Comparison between the control and CAP_{PZ2} treatment groups was achieved using the Student's t-test, and $p < 0.05$ was defined as statistically significant ($*p < 0.05$; $**p < 0.01$; and $***p < 0.001$).

Results

CAP_{PZ2} treatment duration-dependently inhibited proliferation and reduced viability of HT29 and A549 cells

The effect of CAP_{PZ2} (Tinsley and Harris, 2020) on cell viability and cell proliferation was measured using CCK8 assay. As the duration of plasma treatment increased (from 15 to 120 s), the viability of both HT29 (Figure 2B) and A549 (Figure 2C) cells decreased, exhibiting a duration-dependent manner. Using the current plasma parameters, most cancer cells had died by the end of 2 min plasma exposure. In addition, there appeared to be obvious morphological change in the tested tumor cells under phase contrast microscopy examination (Figure 2A). When the cells were exposed under CAP for 30 s, they looked more shrunk and less adherent to the cell culture dish, comparing to those before the plasma treatment. After the treatment duration was doubled, the HT29 and A549 cells became spherical and shriveled, and visually suspended in the cell culture medium, suggesting more prominent cell detachment.

CAP_{PZ2} treatment decreased the migration and invasion of colorectal and lung tumor cell *in vitro*

The effect of CAP_{PZ2} on the *in vitro* tumor cell migration and invasion was investigated using the Transwell migration and Matrigel invasion assay, respectively. Under light microscope, the crystal violet stained HT29 cells (Figure 3A) and A549 cells (Figure 3B) both demonstrated reduced motility after plasma treatment. Plasma-induced suppression on the invasive and
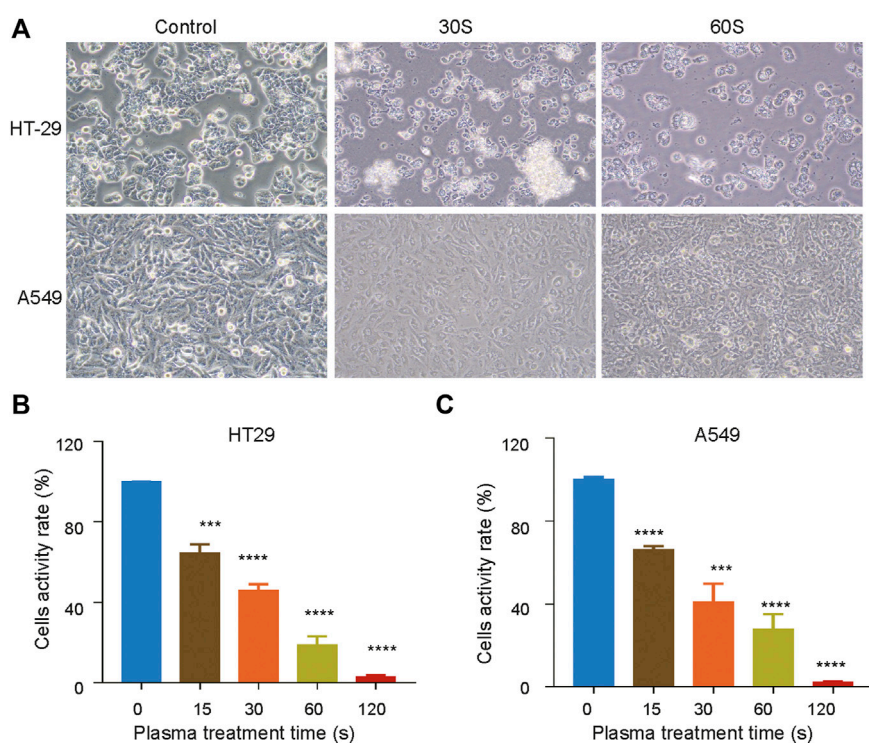
FIGURE 2
Inhibition of cell proliferation by CAP$_{PZ2}$ treatment. **(A)** Optical images of the HT29 and A549 cellular damage caused by CAP$_{PZ2}$ treatment. **(B, C)** Cell activity decreases while CAP$_{PZ2}$ treatment duration increases. The above images and values represent results from three independent experiments and expressed as mean $\pm$ SD. *$p < 0.05$ was considered statistically significant.

migratory capability of these cancer cells seemed to be more dramatic as treatment duration increased from 30 to 60 s.

As shown in Figures 3C,D, CAP$_{PZ2}$ treatment significantly decreased metastatic gene expression in HT29 and A549 cells. Specifically, mRNA expression of *MMP9*, *MMP2*, *VEGF* and *MTDH* in HT29 cells decreased after 30 and 60 s CAP$_{PZ2}$ treatment as a time dependent when compared to the untreated control (Figure 3C). A time dependent downregulation was observed for the expressions of genes *MMP2* and *MTDH* in A549 cells as well. In addition, the expressions of genes *MMP9* and *VEGF* were also downregulated after 30 s CAP treatment in A549 cells (Figure 3D).

CAP$_{PZ2}$ treatment induced apoptosis in HT29 and A549 cells

Apoptosis is a form of programmed cell death, which occurs in physiological and pathological conditions (Lv et al., 2008). In addition, apoptosis plays a pivotal role in tumorigenesis, tumor metastasis, and resistance to antineoplastic medications.

Therefore, inducing apoptotic cell death is a promising strategy to prevent and treat cancer. In order to understand the mechanism of plasma-induced growth inhibition, the HT29 and A549 cells treated with CAP$_{PZ2}$ were nuclei-stained and observed under fluorescent microscopy. As Figure 4A demonstrated, cells that were exposed to CAP$_{PZ2}$ (15, 30 and 60 s) all had condensation of chromatin and appearance of apoptotic bodies, whereas untreated cells exhibited a typically non-adherent and round morphology. In order to gain further insight into the antiproliferative effect of CAP$_{PZ2}$, transmission electron microscopy (TEM) was used to obtain ultrastructural information (Figure 4B). After the HT29 and A549 cells were treated with CAP$_{PZ2}$ for 30 s, the TEM images discovered membrane damage, such as cell membrane blistering, nuclear membrane atrophy and irregular shape. In addition, there were chromatin condensation and nuclear fragmentation in the nuclei, as well as vacuolization and abnormal increase of mitochondria in the cytoplasm.

In addition to the above qualitative assessment, quantitative analysis of cellular apoptosis after CAP$_{PZ2}$ treatment was conducted using flow cytometry. As shown in Figure 5A, PE annexin-V positive cells were considered as populations in the
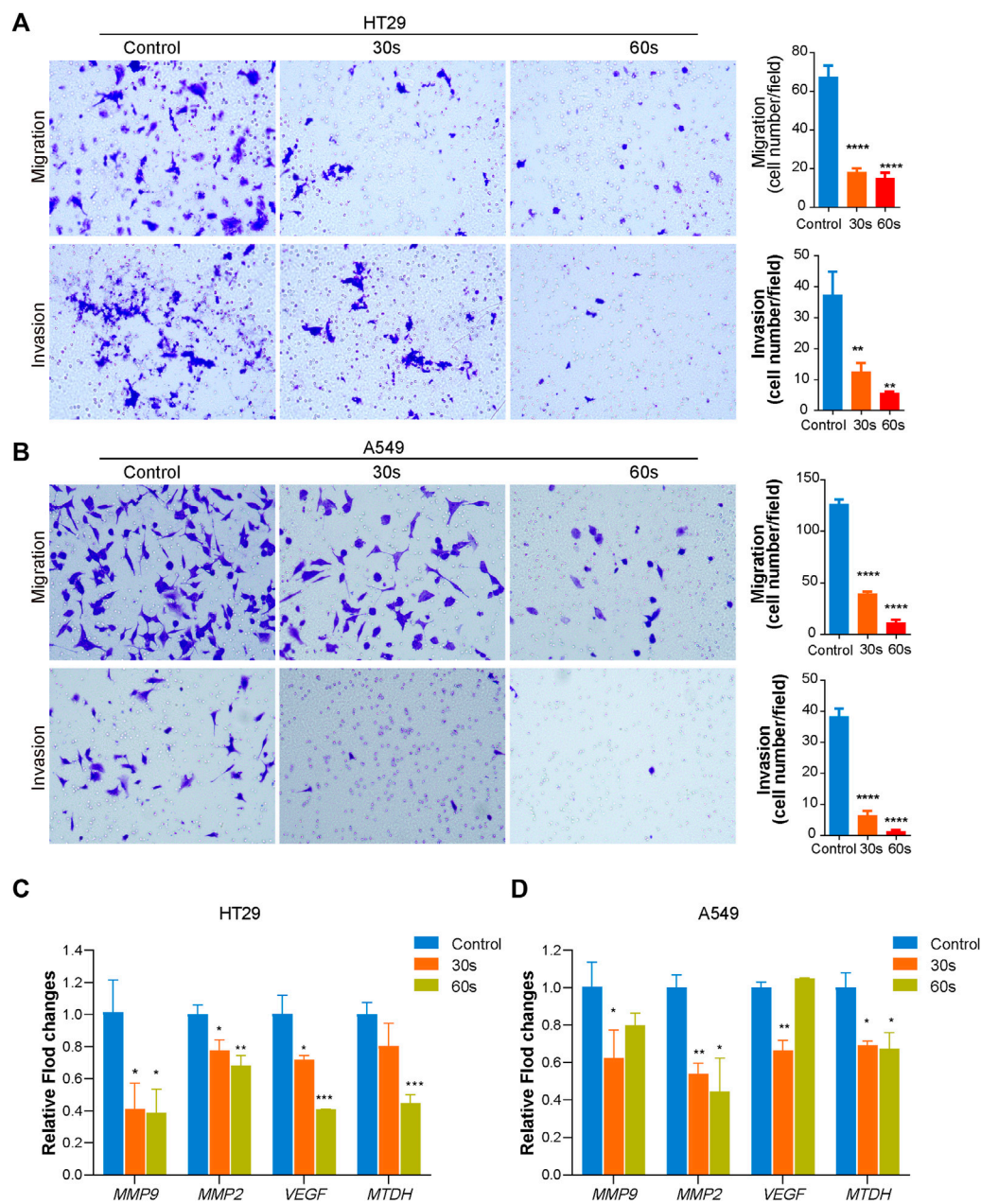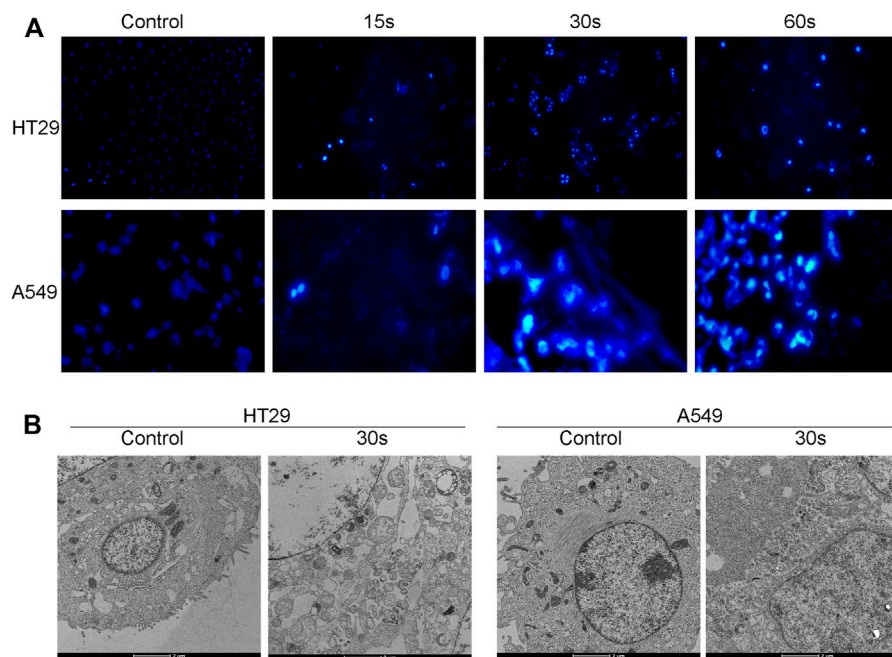
FIGURE 3
Effect of CAP$_{PZ2}$ treatment on the migratory and invasive ability of the HT29 and A549 cells. The HT29 **(A)** and A549 **(B)** cells were treated by CAP$_{PZ2}$ for 30 and 60 s, incubated for 24 h, before subjected to Transwell migration and Matrigel invasion assays. Representative images (left) and statistics (right) of migration and invasion assay were shown. The scale bar equals 200 μm. The experiments were performed in triplicates. **(C,D)** mRNA (*MMP9, MMP2, VEGF, MTDH*) expression changes during CAP$_{PZ2}$ treatment with different time. *$p < 0.05$, **$p < 0.01$, and ***$p < 0.001$ versus control, $n = 3$.

early and late apoptosis. CAP$_{PZ2}$ induced a significantly increased population of apoptotic HT29 and A549 cells when compared with the negative control. This plasma-induced increase in the apoptosis rate seemed to be in a plasma dose-dependent manner (Figure 5B). This change in apoptosis was

further evaluated through AO/EB staining. The HT29 and A549 cells were stained by AO/EB and analyzed using fluorescent microscopy (Figure 5C). Acridine orange is a vital dye that stains both living and dead cells, whereas ethidium bromide only stains cells that have lost their membrane integrity.

FIGURE 4
Qualitative analysis of the HT29 and A549 cellular apoptosis upon CAP$_{PZ2}$ treatment. **(A)** Fluorescent microscopic images of nuclear changes (e.g., chromatin condensation) in the HT29 and A549 cells stained with Hoechst33342. **(B)** Transmission electron microscopic images of ultrathin sections (x10,000) demonstrating subcellular changes in the HT29 and A549 cells treated with CAP$_{PZ2}$ for 30 s. All images are at the same magnification.

Living cells turn green and can thus be distinguished from apoptotic cells (Ralph et al., 2016; Aranha et al., 2021). After treatment with CAP$_{PZ2}$ for 30 and 60 s, a significant decrease in the viability of HT29 and A549 cells was detected, while the number of apoptotic cells increased after 30 and 60 s of plasma treatment. Collectively, these results indicate that tumor cell death after CAP$_{PZ2}$ treatment occurred mainly through enhanced apoptosis.

CAP$_{PZ2}$ treatment raised intracellular reactive oxygen species accumulation

The release of reactive oxygen species (ROS) by most apoptosis inducers is considered the key mediator of apoptosis signaling transduction (Negrin et al., 2010). Since increased ROS production in tumor cells may lead to the activation of mitochondrial pathways and cell death, we decided to investigate whether ROS are involved in CAP$_{PZ2}$-induced apoptosis. As shown in Figure 6, the HT29 and A549 cells exposed to CAP$_{PZ2}$ (30 and 60 s) exhibited a significantly enhanced accumulation of intracellular ROS (Figures 6A,B). When compared to untreated cells, the HT29 and A549 cells treated with 30 and 60s of CAP$_{PZ2}$ demonstrated notable increase of

fluorescence emitted by the ROS-induced oxidation of DCFH-DA (Figures 6C,D).

Potential molecular pathway of plasma-induced apoptosis in HT29 and A549 cells

In order to establish whether CAP$_{PZ2}$ induces apoptosis through the mitochondrial pathway, we performed Western blot on relevant proteins that are differentially expressed by the HT29 and A549 cells treated with or without CAP$_{PZ2}$. Firstly, as shown in Figures 7A–D, CAP$_{PZ2}$ greatly increased the protein expression level of cytosol cytochrome-c when compared with the control group. Cytochrome-c is one of the most prominent actors in the apoptotic scene. Secondly, in order to further address the apoptotic effect of CAP$_{PZ2}$ on the HT29 and A549 cells, we analyzed the levels of cleaved caspase-3, caspase-9 and cleaved PARP. PARP, a substrate of caspase-3, is an early hallmark of apoptosis. After plasma treatment for 30 and 60 s, the amount of cleaved PARP elevated with increasing plasma dose of CAP$_{PZ2}$ treatment. The production of cleaved caspase-3 and caspase-9 also increased significantly in a plasma dose-dependent manner in the HT29 and A549 cells treated with CAP$_{PZ2}$. Lastly, in order to investigate the molecular events involved in CAP$_{PZ2}$-induced
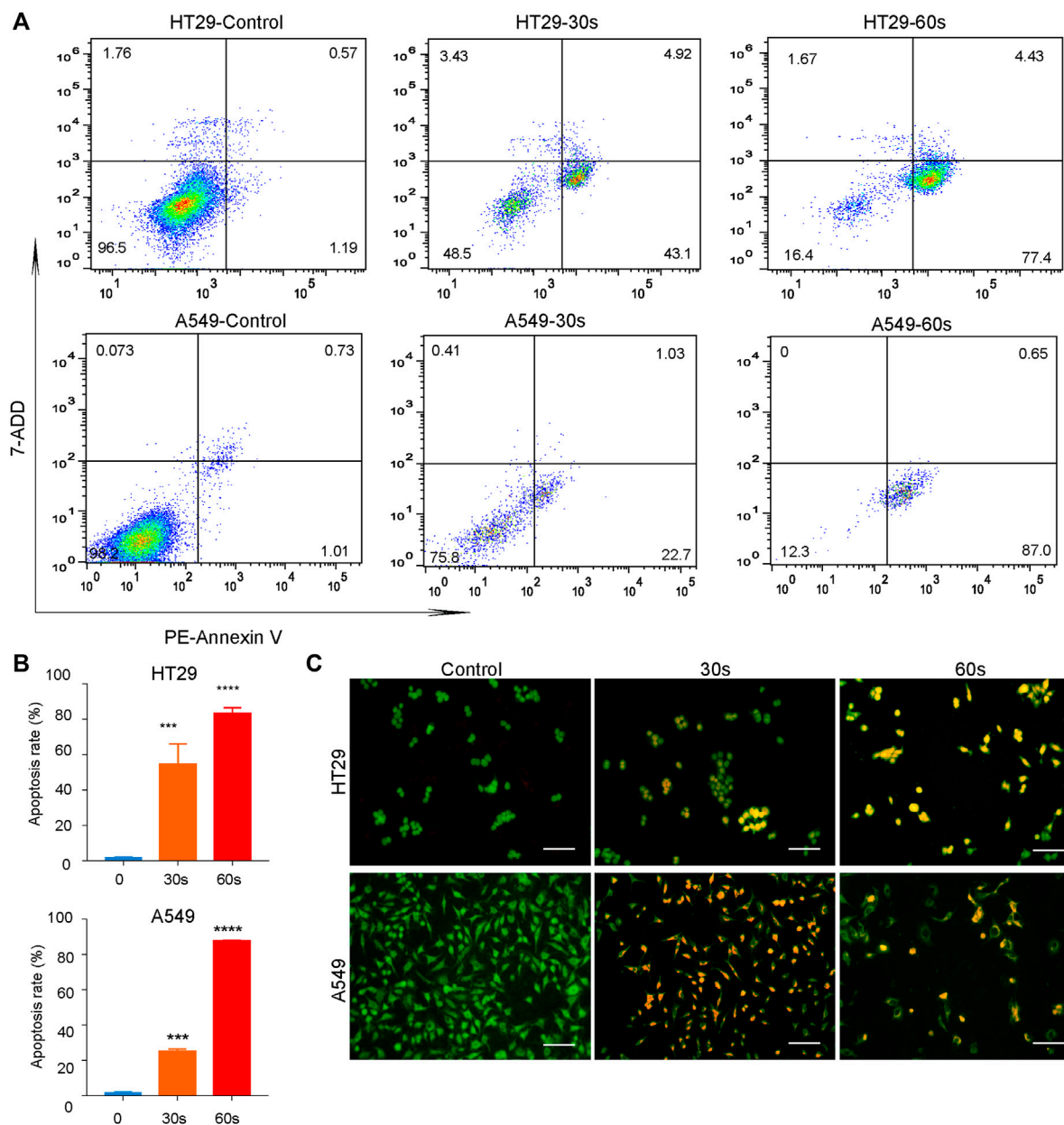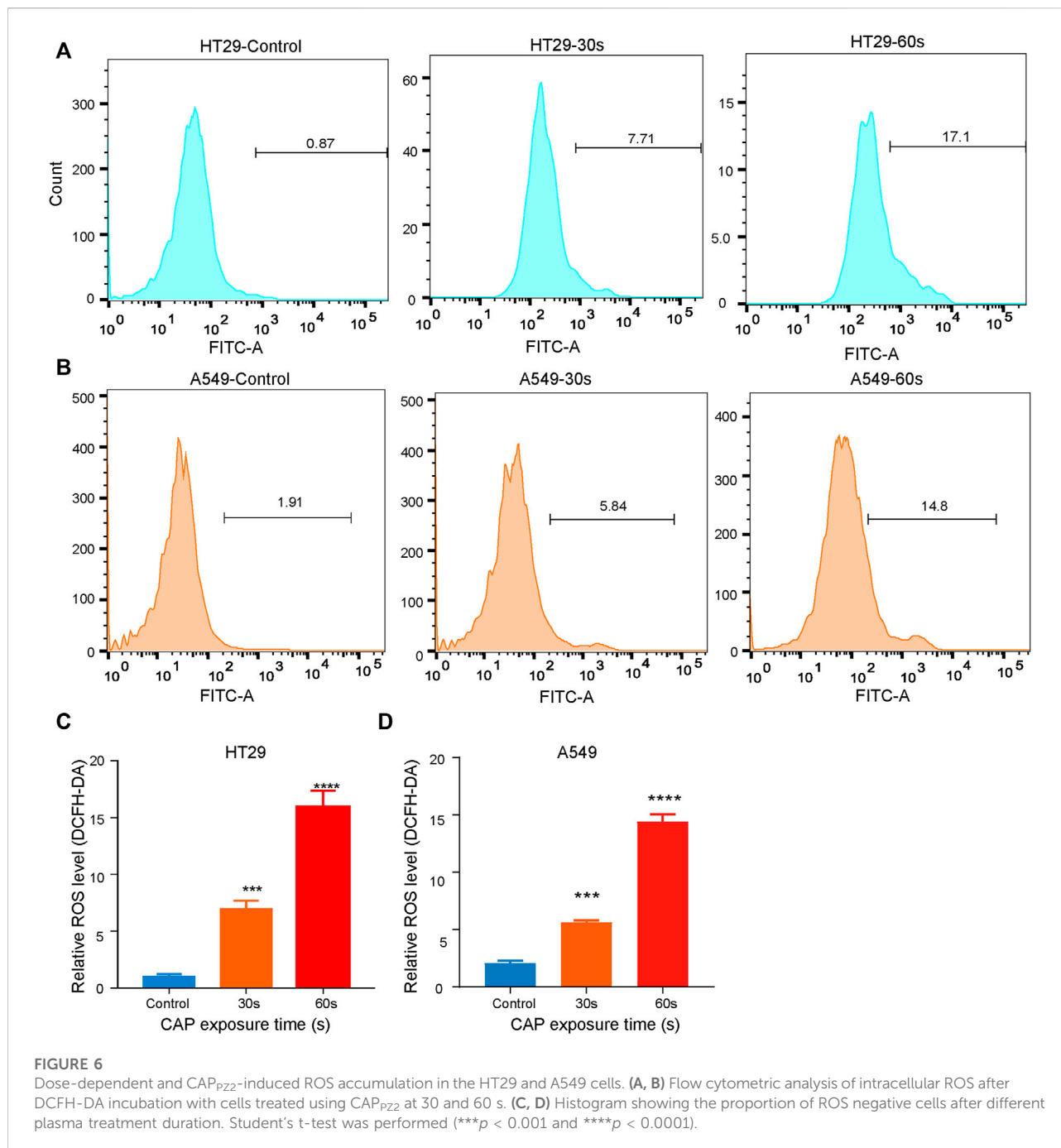
FIGURE 5
Quantitative analysis of the HT29 and A549 cellular apoptosis upon CAP$_{PZ2}$ treatment. **(A)** Flow cytometric screening of the HT29 and A549 cells treated by CAP$_{PZ2}$ for 30 and 60 s. PE Annexin-V/7-ADD staining was used to measure apoptosis rate. The proportion of cells in each quadrant are marked on the figures. **(B)** Histogram of the corresponding apoptosis rate expressed as mean $\pm$ SD of three independent experiments (***$p <$ 0.001 and ****$p <$ 0.0001). **(C)** Fluorescence microscopic images of the apoptotic HT29 and A549 cells detected using AO/EB staining. Green represents viable cells and orange represents apoptotic cells.

apoptosis, expression of the Bcl-2 and Bax rheostat that regulates antioxidant pathway and cell death was also assessed using Western blotting. The results showed that the expression of anti-apoptotic protein Bcl-2 was plasma dose-dependently decreased in the CAP$_{PZ2}$ groups, whereas that of pro-apoptotic protein Bax was increased accordingly (Figure 7).

CAP$_{PZ2}$ treatment inhibited *in vivo* tumor growth in a xenograft mouse model

In order to verify the anti-neoplastic effect of CAP$_{PZ2}$ *in vivo*, we performed a proof-of-principle experiment using a mouse xenograft model incorporating the HT29 or A549 cells

FIGURE 6
Dose-dependent and CAP$_{PZ2}$-induced ROS accumulation in the HT29 and A549 cells. **(A, B)** Flow cytometric analysis of intracellular ROS after DCFH-DA incubation with cells treated using CAP$_{PZ2}$ at 30 and 60 s. **(C, D)** Histogram showing the proportion of ROS negative cells after different plasma treatment duration. Student's t-test was performed (***$p < 0.001$ and ****$p < 0.0001$).

(Figures 8A,B). The results collectively showed that the tumor growth was significantly suppressed in the CAP$_{PZ2}$ treatment group. The qualitative photos of the excised tumors demonstrated that plasma-irradiated tumors appeared to be smaller than the untreated specimens (Figure 8C), especially at time points towards the end of experiment. On the other hand, the quantitative tumor measurement revealed that while the *in-situ* cancer grew steadily over time in the untreated group, tumor growth in the plasma-treated group

appeared much slower in comparison (Figure 8D). The tumor volume in the A549 cells inoculated mice was virtually unchanged in the first few weeks. In addition, at a chose time point, the average tumor weight was significantly lower in the CAP$_{PZ2}$-treated mice (Figure 8E).

In order to explore and verify the possible molecular mechanism involved in the *in vivo* oncological CAP$_{PZ2}$ treatment, the expression of apoptosis-related proteins, such as cytochrome-*c*, cleavage-PARP, cleaved caspase-3, Bcl-2, Bax
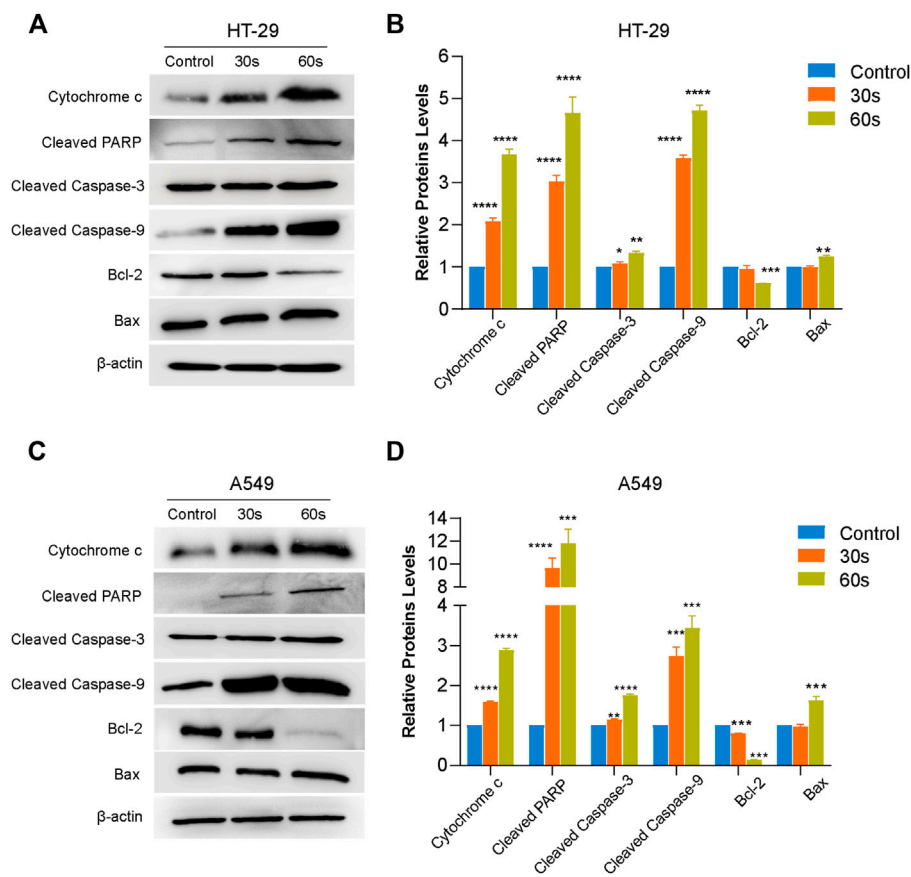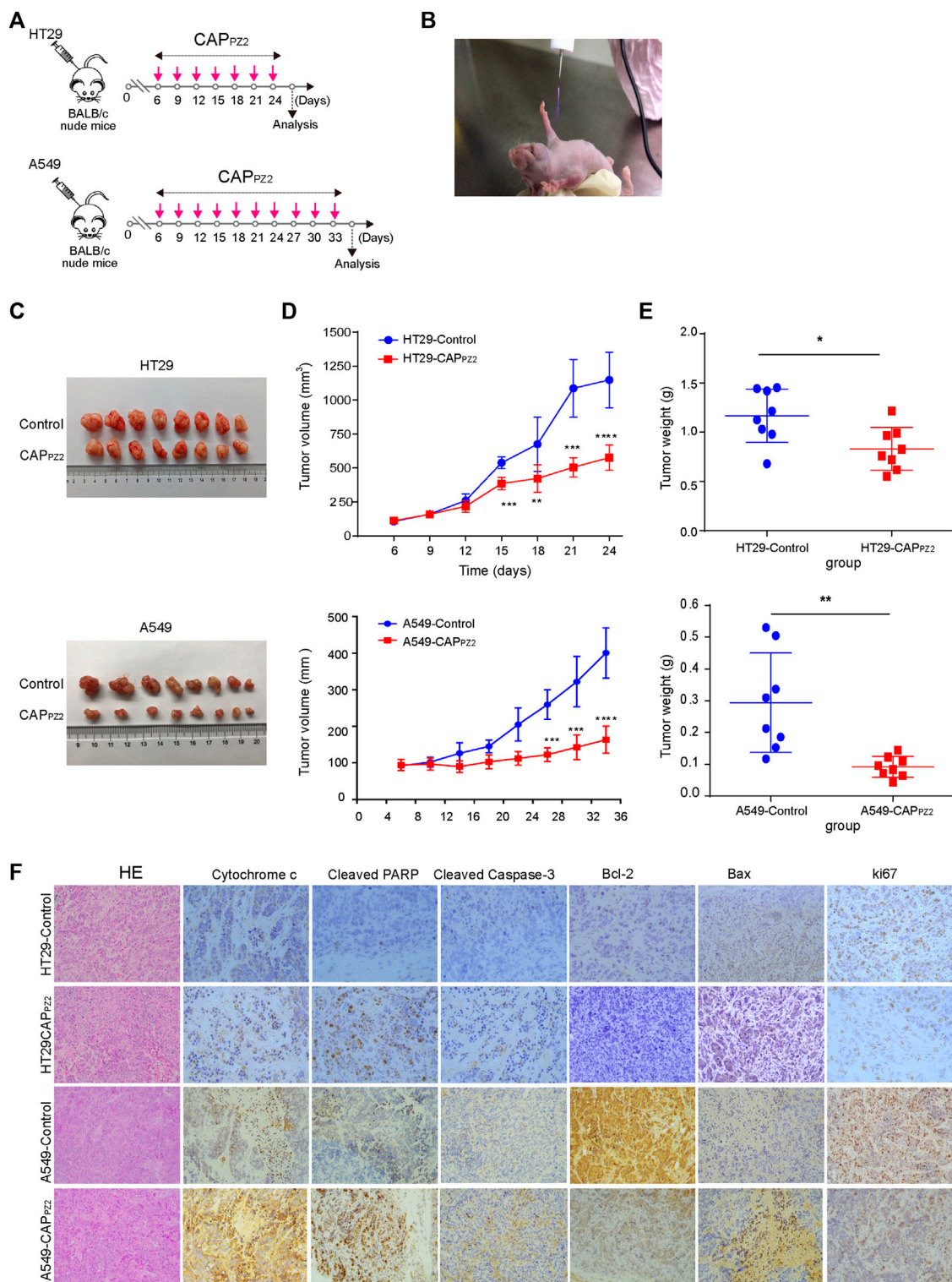
FIGURE 7
Western blot analysis revealing the potential signaling pathway of plasma-induced apoptosis in the HT29 and A549 cells treated using CAP$_{PZ2}$. Proteins were extracted from the HT29 **(A,B)** and A549 **(C,D)** cells upon treatment by CAP$_{PZ2}$ for 30 and 60 s, and subjected to Western blotting using the respective antibodies with β-actin antibody acting as a parallel blotting.*$p < 0.05$, **$p < 0.01$, ***$p < 0.001$ and ****$p < 0.0001$ versus control, $n = 3$.

and ki67 proteins in the CAP$_{PZ2}$-treated and control samples was analyzed using immunohistochemical staining. In our study, microscopic examination showed that the percentage of cytochrome-c, cleavage-PARP, cleaved caspase-3 and Bax positive cells was higher in the CAP$_{PZ2}$-treated group compared to the control (Figure 8F). The apoptosis-promoting effect of CAP$_{PZ2}$ was further confirmed by the results generated by IHC staining of Bcl-2. Majority of tumors from the control group showed moderate to strong staining intensity of Bcl-2, whereas the CAP$_{PZ2}$-treated tumors presented weak or undetectable Bcl-2 expression (Figure 8F). This coincided with the reduction in tumor growth as indicated by the Ki67 staining. These results collectively revealed that the CAP$_{PZ2}$-induced tumor inhibition may be through promotion of apoptosis, which is in line with the activation of cytochrome-c, PARP, cleaved caspase-3 and Bax, as well as downregulation of Bcl-2 and ki67 in the CAP$_{PZ2}$-treated tumor samples.

Discussion

Cancer is the leading cause of death in the developed countries and the second leading in the developing world. However, the non-surgical treatment options for solid malignant tumors have remained limited over the recent decades. Therapeutic modalities, such as radiation, chemotherapy, immunotherapy, administered alone or in combination, all have suboptimal therapeutic effects. Cold atmospheric plasma has emerged as a promising antineoplastic adjunct in recent years (Ratovitski et al., 2014). There have been copious preclinical and clinical reports pertaining CAP's oncological application in various types of cancer, such as cutaneous, breast, liver, ovarian, pancreatic, oral, and thyroid cancers (Chang et al., 2014a; Chang et al., 2014b; Gay-Mimbrera et al., 2016; Dai et al., 2018). CAP essentially refers to a partially ionized gas containing reactive oxygen and nitrogen species, ions and electrons, and ultraviolet

FIGURE 8

In vivo CAP$_{PZ2}$ treatment of mouse xenograft tumors. **(A)** Flowchart of *in vivo* CAP$_{PZ2}$ therapy regimen. **(B)** Photograph of an operating Piezobrush® PZ2 CAP device irradiating tumors on a nude mouse bearing the HT29 or A549 cells. **(C)** Pathological specimens of resected *in situ* tumors with and without CAP$_{PZ2}$ treatment. **(D)** Tumor growth curves of mice xenografts during the entire course of CAP$_{PZ2}$ treatment. **(E)** Tumor weight after the last dose of plasma administration (*$p < 0.05$, **$p < 0.01$, ***$p < 0.001$, $n = 8$). **(F)** Representative histological images characterizing tumours and Immunohistochemical analysis using antibodies against various apoptosis-related proteins. Scale bar = 50 µm.

photons. This combination can bring physicochemical cues to biological targets without causing thermal damage to adjacent healthy recipients (Adhikari et al., 2019).

Although the mechanistic exploration of plasma oncology is still at a relatively early stage, several cellular events and molecular pathways have been discovered and proposed (Semmler et al., 2020). Previous studies have confirmed that appropriate dose of CAP usually does not cause cell necrosis, but rather sublethal or lethal cellular reactions (e.g., detachment and apoptosis) in various cell types (Wang et al., 2011; Adhikari and Arora, 2015; Zhu et al., 2016). Normal tissue homeostasis and cell function are maintained by the balance between proliferation and apoptosis (Wang et al., 2012). Cancer is a typical disease in which malignant cell clones escape this equilibrium and improperly proliferate without compensatory apoptosis (Kim et al., 2007). In other words, premalignant cells grow faster than normal cells do because of the imbalance of cell growth and cell death mechanisms. Therefore, the success of a cancer treatment largely depends on the degree to which they preferentially induce tumor cell death while allowing normal tissue to survive.

According to the latest global cancer burden data released by the International Agency for Research on Cancer under WHO in 2020, the incidence rate of lung cancer and colon cancer ranks top two and three, with the former still being the most lethal cancer worldwide. Therefore, we used colon cancer cells HT29 and lung cancer cells A549 as the *in vitro* experimental model in this study. Our preliminary results showed that CAP_{PZ2} treatment inhibited proliferation of the above cells in a plasma dose-dependent manner and caused morphological changes, such as cell shrinkage, chromatin condensation and nuclear fragmentation. These results are consistent with independent studies from other research groups using different cancer cell models (Xia et al., 2019; Bekeschus et al., 2020).

Cancer cell invasion and migration are the major differentiating features of malignant tumors from benign ones. They are also one of the important causes of treatment failure. Thus, preventing migration and invasion of cancer cells and associated tumor metastasis is a hotspot in cancer research. Cancer cell migration is usually regulated by adhesion receptors, matrix-degrading enzymes, and cell-cell adhesion molecules. However, even cancer therapeutics specifically targeting these regulators sometimes prove ineffective in clinical trials, mainly because cancer cells can modify their migrative mechanism in response to various conditions (Friedl and Wolf, 2003). Fortunately, plenty of studies have shown that CAP treatment can effectively inhibit tumor invasion and metastasis, which provides a novel strategy for cancer therapy (Chang et al., 2014b; Li et al., 2016). Our results were consistent with other reports (Kang et al., 2017), since the migration and invasion of HT29 and A549 cells were significantly inhibited by CAP_{PZ2} treatment. MMP9 and MMP2 have similar biological function and they play a key role in the decomposition of extracellular matrix. During the development of cancer,

MMP9 and MMP2 degrade the basement membrane and promote the metastasis of tumor cell to distant tissues and/or organs. VEGF is a protein that stimulates the growth and formation of the circulatory system and blood vessels (angiogenesis and angiogenesis). Regarding its role in cancer, VEGF promotes the presence of nutrients and oxygen in cancer cells. More blood supply promotes cancer cell proliferation and inhibits apoptosis. Therefore, downregulation of VEGF expression could be used as an indicator of inhibiting tumor progression. A more direct indicator of cancer progression, MTDH is an oncogene which promotes cancer cell proliferation. Moreover, MTDH is attributed to the development of chemoresistance as well as increasing metastatic potential. In our study, we found CAP_{PZ2} treatment downregulated all four markers in HT29 and A549 cells. In addition, since ROS are considered to have important roles during cancer cell migration and invasion (Tochhawng et al., 2013), and CAP happens to generate extracellular and intracellular ROS, further study to explore the role of plasma-mediated redox balance for CAP's anti-invasion and anti-migration effects are warranted.

Our further study exploring the cellular events underlying CAP's inhibitory effect on HT29 and A549 cell proliferation discovered that the main contributing factor is increased rate of early apoptosis and late apoptosis in these cells after plasma treatment. These results were consolidated by morphological signs of apoptosis under microscopic observation. Other studies have also reported similar findings on CAP's antiproliferative effect and CAP-induced apoptosis (Zhong et al., 2016; Gan et al., 2019). Apoptosis, the process of programmed cell death, plays a pivotal role in the pathogenesis of many diseases. Apoptosis is characterized by distinct morphological features and regulated by a series of biochemical events leading to cell death (Elmore, 2007). Cancer is one of the situations where too little apoptosis happens, leading to reduced death in malignant cells. Mechanistic insights into the impact of CAP-induced apoptosis have been a hot area of research in plasma oncology.

Recent studies revealed that CAP can trigger RONS-based tumor cell apoptosis (Bauer et al., 2019). RONS has been shown to induce various biological processes, including apoptosis. This means that the redox state of cells is a key factor to determine their sensitivity to apoptotic stimulation (Chen et al., 2015). Low concentration of ROS plays a role of intracellular messenger in many molecular events, such as cell proliferation, whereas high density of ROS contributes to cell apoptosis. Our results demonstrated a dramatic burst of ROS in a plasma dose-dependent fashion after CAP_{PZ2} treatment, suggesting that ROS generation is involved in the CAP_{PZ2}-induced apoptosis in HT29 and A549 cells. Dezest et al. (2017) found that the proteasome, a crucial intracellular proteolytic system which modulate tumor cell growth and survival, is a target of CAP. Interestingly, in addition to RONS, plasma-generated charged

particles and electromagnetic emission also play an important role in cancer cell death (Yan et al., 2020).

Since we have depicted the cellular events and intracellular chemical cues involved in the *in vitro* cancer treatment by CAP, we performed further study to explore the potential molecular pathway during CAP$_{PZ2}$-induced apoptosis. Apoptosis can be initiated by a death receptor-mediated pathway or a mitochondria-mediated pathway (Wang et al., 2014). In the mitochondria-mediated pathway, cytochrome *c* is released from mitochondria to cytoplasm due to the change of mitochondrial membrane permeability. The ROS produced by CAP treatment triggers molecular signaling pathways and promotes mitochondrial disturbance, resulting in apoptosis (Ahn et al., 2014). To further assess the anti-tumor mechanism of CAP$_{PZ2}$, we discovered that CAP$_{PZ2}$ treatment greatly increased cytochrome *c* in cytosol of HT29 and A549 cells, suggesting that the intrinsic apoptosis route *via* mitochondria is involved. Once cytochrome *c* is released, it forms apoptotic bodies with Apaf-1 and procaspase-9 in the presence of dATP, leading to activation of caspase-9. Caspases play an important role in the executive stage of apoptosis (Wang et al., 2012). In the death receptor-mediated pathway, caspase-9 is activated downstream of the death-inducing signaling complex. The active caspase-9 activates downstream caspase-3, which leads to activation of the mitochondrial pathway (Cooper et al., 2007). The effector caspases may cleave a number of structural and regulatory cellular proteins including PARP and lamin protein, and are responsible for the typical morphological and biochemical features of an apoptotic cell (Bossy-Wetzel and Green, 1999).

The mitochondrial pathway is one of the most important cellular apoptosis signal transduction pathways, and Bcl-2 family is a key regulatory factor of this pathway. It can alter the balance between pro-apoptotic and anti-apoptotic pathway in tumor cells, determine the response of cells to external stimuli, and thus determine the fate of cells (Turrini et al., 2017). As an anti-apoptotic factor, Bcl-2 maintains the integrity of mitochondrial membrane, while Bax promotes apoptosis by destroying the mitochondrial membrane (Antonsson, 2004). Our results showed that the effect of CAP$_{PZ2}$ treatment did cause these events through apoptosis, as CAP$_{PZ2}$ markedly elevated the expression of cleaved form of PARP, caspase-3, and caspase-9. Moreover, we have also found an increase in the expression of Bax protein and a decrease in the expression of Bcl-2 in HT29 and A549 cells treated using CAP$_{PZ2}$. An increase in the ratio of Bax/Bcl-2 stimulates the release of cytosolic cytochrome *c*, leading to the activation of caspase-3 and PARP. These results further confirmed that CAP$_{PZ2}$ oncotherapy can promote apoptosis of the HT29 and A549 cells through caspase-3 modulation *via* the mitochondrial pathway.

The number of other mechanistic studies exploring the molecular pathway of plasma-induced cancer cell apoptosis

are still limited. Xia et al. (2019) reported that CAP induces apoptosis of melanoma cells *via* Sestrin2-mediated nitric oxide synthase signalling. Haralambiev et al. (2020) discovered that CAP treatment of osteosarcoma cells resulted in suppressed cell growth, activation of caspase-3/caspase-7 and degradation of genomic DNA. This apoptotic effect seemed independent of the plasma devices used. Yang et al. (2020) demonstrated that CAP-activated solution induces apoptotic signaling in basal cell carcinoma cells, and that this effect was associated with the activation of the MAPK signaling pathway. Finally, Estarabadi et al. (2021) found that both direct and indirect CAP treatment could not only induce cytotoxicity by shifting Bax/Bcl-2 towards apoptosis, but also cause genotoxicity in oesophageal cancer cells. Although there has been research reporting that synergistic treatment using CAP and silymarin nanoemulsion could inhibit melanoma tumorigenesis *via* targeting HGF/c-MET downstream pathway (Adhikari et al., 2019), our discussion here is limited to standalone CAP treatment. Over the last several years, a mainstay and goal of clinical plasma oncology has been the exploration of the mechanism of plasma-triggered cancer cell apoptosis. However, this is facing considerable challenge partially because the interaction of apoptosis pathways with other signalling mechanisms can also affect cell death. Once we have gained better understanding in this area of research, CAP has the potential to serve as a customizable adjuvant therapy for various types of cancer.

As we have successfully applied CAP$_{PZ2}$ treatment *in vitro* for lung cancer and colon cancer cells, we furthered our work by exploring its therapeutic potential using cell-derived xenograft (CDX) models in animals. Our results showed that CAP$_{PZ2}$ could significantly inhibit the growth of tumors *in vivo*. Immunohistochemically, in the tumors developed in these mice, the percentages of cytochrome-*c*, cleavage-PARP, and cleaved caspase-3 positive cells were higher in the CAP$_{PZ2}$-treated group. Further results on Bax/Bcl-2 coincided with the reduction in tumor growth as indicated by the Ki67 staining. In other word, it is most likely that the anticancer effect on HT29 or A549 cells xenografted mice was also due to CAP$_{PZ2}$-induced apoptosis through the mitochondrial pathway. So far, the CAP induced-apoptosis studies using various cancer cell lines *in vitro* vastly outnumber those using *in vivo* models. Our near future plan includes establishing patient-derived xenograft (PDX) models for oncological purpose in plasma medicine. Our ultimate objective is to contribute to developing a versatile and effective CAP-based oncotherapy after meticulous clinical trials.

Conclusion

In this preclinical study, we are the first to demonstrate universal anti-tumor effect on lung cancer and colon cancer cells models using cold atmospheric plasma. A handheld piezoelectric

direct discharge CAP device, Piezobrush® PZ2, was used throughout this work. The anti-proliferative effect of CAP$_{PZ2}$ was established using human colorectal adenocarcinoma HT29 cells and human lung adenocarcinoma A549 cells *in vitro*. At the cellular level, CAP$_{PZ2}$ treatment induced cancer cell apoptosis, inhibited tumor cell migration and invasion, and changed the morphological integrity and stability of mitochondria. At the protein and molecular level, CAP shifted the expression of apoptosis-related markers, such as Bcl-2, Bax, Cyt *c*, and caspase-3, towards the anti-apoptotic exit. On the other hand, the antineoplastic effect of CAP was confirmed *in vivo* using cell-derived xenograft animal models. The immunohistochemical analysis again revealed activation of Cyt *c*, PARP, cleaved caspase-3 and Bax, and suppression of Bcl-2 and ki67 in the plasma-treated specimens, which is consistent with *in vitro* results. Collectively, we revealed that CAP$_{PZ2}$ could induce apoptosis of lung cancer and colon cancer cells *in vitro* and *in vivo* through the mitochondrial pathway.

Data availability statement

The original contributions presented in the study are included in the article/Supplementary Material, further inquiries can be directed to the corresponding author.

Ethics statement

The animal study was reviewed and approved by Experimental Animal Ethics Committee of Tongji University. Written informed consent was obtained from the owners for the participation of their animals in this study.

Author contributions

Conceptualization, FT and YW; methodology, YW, XM, and XL; writing-original draft preparation, YW; writing-review and editing, YW and FT; supervision, ZC and FT; funding acquisition, YW, ZC, and FT. All authors have read and agreed to the published version of the manuscript. The authors declare no conflict of interest.

Conflict of interest

The authors declare that the research was conducted in the absence of any commercial or financial relationships that could be construed as a potential conflict of interest.

Publisher's note

All claims expressed in this article are solely those of the authors and do not necessarily represent those of their affiliated organizations, or those of the publisher, the editors and the reviewers. Any product that may be evaluated in this article, or claim that may be made by its manufacturer, is not guaranteed or endorsed by the publisher.

Supplementary material

The Supplementary Material for this article can be found online at: https://www.frontiersin.org/articles/10.3389/fcell.2022.915785/full#supplementary-material

References

Adhikari, M., and Arora, R. (2015). Nano-silymarin provides protection against gamma-radiation-induced oxidative stress in cultured human embryonic kidney cells. *Mutat. Res. Genet. Toxicol. Environ. Mutagen.* 792, 1–11. doi:10.1016/j.mrgentox.2015.08.006

Adhikari, M., Kaushik, N., Ghimire, B., Adhikari, B., Baboota, S., Al-Khedhairy, A. A., et al. (2019). Cold atmospheric plasma and silymarin nanoemulsion synergistically inhibits human melanoma tumorigenesis via targeting HGF/c-MET downstream pathway. *Cell Commun. Signal.* 17, 52. doi:10.1186/s12964-019-0360-4

Ahn, H. J., Kim, K. I., Hoan, N. N., Kim, C. H., Moon, E., Choi, K. S., et al. (2014). Targeting cancer cells with reactive oxygen and nitrogen species generated by atmospheric-pressure air plasma. *Plos One* 9, e86173. doi:10.1371/journal.pone.0086173

Ahn, H. J., Kim, K. I., Kim, G., Moon, E., Yang, S. S., Lee, J. S., et al. (2011). Atmospheric-Pressure plasma jet induces apoptosis involving mitochondria via generation of free radicals. *Plos One* 6, e28154. doi:10.1371/journal.pone.0028154

Antonsson, B. (2004). Mitochondria and the Bcl-2 family proteins in apoptosis signaling pathways. *Mol. Cell. Biochem.* 256, 141–155. doi:10.1023/B:Mcbi.0000009865.70898.36

Aranha, E. S. P., Portilho, A. J. D., Sousa, L. B. D., Silva, E. L. D., Mesquita, F. P., Rocha, W. C., et al. (2021). 22 beta-hydroxytingenone induces apoptosis and suppresses invasiveness of melanoma cells by inhibiting MMP-9 activity and MAPK signaling. *J. Ethnopharmacol.* 267, 113605. doi:10.1016/j.jep.2020.113605

Arndt, S., Unger, P., Wacker, E., Shimizu, T., Heinlin, J., Li, Y. F., et al. (2013). Cold atmospheric plasma (CAP) changes gene expression of key molecules of the

wound healing machinery and improves wound healing *in vitro* and *in vivo. Plos One* 8, e79325. doi:10.1371/journal.pone.0079325

Aryal, S., and Bisht, G. (2017). New paradigm for a targeted cancer therapeutic approach: a short review on potential synergy of gold nanoparticles and cold atmospheric plasma. *Biomedicines* 5, E38. doi:10.3390/biomedicines5030038

Bauer, G., Sersenová, D., Graves, D. B., and Machala, Z. (2019). Cold atmospheric plasma and plasma-activated medium trigger RONS-based tumor cell apoptosis. *Sci. Rep.* 9, 14210. doi:10.1038/s41598-019-50291-0

Bekeschus, S., Moritz, J., Helfrich, I., Boeckmann, L., Weltmann, K.-D., Emmert, S., et al. (2020). *Ex vivo* exposure of human melanoma tissue to cold physical plasma elicits apoptosis and modulates inflammation. *Appl. Sci.* 10, 1971. doi:10.3390/app10061971

Binenbaum, Y., Ben-David, G., Gil, Z., Slutsker, Y. Z., Ryzhkov, M. A., Felsteiner, J., et al. (2017). Cold atmospheric plasma, created at the tip of an elongated flexible capillary using low electric current, can slow the progression of melanoma. *Plos One* 12, e0169457. doi:10.1371/journal.pone.0169457

Bossy-Wetzel, E., and Green, D. R. (1999). Caspases induce cytochrome c release from mitochondria by activating cytosolic factors. *J. Biol. Chem.* 274, 17484–17490. doi:10.1074/jbc.274.25.17484

Chang, J. W., Kang, S. U., Shin, Y. S., Kim, K. I., Seo, S. J., Yang, S. S., et al. (2014a). Non-thermal atmospheric pressure plasma induces apoptosis in oral cavity squamous cell carcinoma: involvement of DNA-damage-triggering sub-G(1) arrest via the ATM/p53 pathway. *Arch. Biochem. Biophys.* 545, 133–140. doi:10.1016/j.abb.2014.01.022

Chang, J. W., Kang, S. U., Shin, Y. S., Kim, K. I., Seo, S. J., Yang, S. S., et al. (2014b). Non-thermal atmospheric pressure plasma inhibits thyroid papillary cancer cell invasion via cytoskeletal modulation, altered MMP-2/-9/uPA activity. *Plos One* 9, e92198. doi:10.1371/journal.pone.0092198

Chen, Y., Liu, J. M., Xiong, X. X., Qiu, X. Y., Pan, F., Liu, D., et al. (2015). Piperlongumine selectively kills hepatocellular carcinoma cells and preferentially inhibits their invasion via ROS-ER-MAPKs-CHOP. *Oncotarget* 6, 6406–6421. doi:10.18632/oncotarget.3444

Cheng, X. Q., Rajjoub, K., Shashurin, A., Yan, D. Y., Sherman, J. H., Bian, K., et al. (2017). Enhancing cold atmospheric plasma treatment of cancer cells by static magnetic field. *Bioelectromagnetics* 38, 53–62. doi:10.1002/bem.22014

Cooper, D. M., Pio, F., Thi, E. P., Theilmann, D., and Lowenberger, C. (2007). Characterization of Aedes dredd: a novel initiator caspase from the yellow fever mosquito, *Aedes aegypti. Insect biochem. Mol. Biol.* 37, 559–569. doi:10.1016/j.ibmb.2007.03.005

Dai, X., Bazaka, K., Richard, D. J., Thompson, E. W., and Ostrikov, K. (2018). The emerging role of gas plasma in oncotherapy. *Trends Biotechnol.* 36, 1183–1198. doi:10.1016/j.tibtech.2018.06.010

Dezest, M., Chavatte, L., Bourdens, M., Quinton, D., Camus, M., Garrigues, L., et al. (2017). Mechanistic insights into the impact of Cold Atmospheric Pressure Plasma on human epithelial cell lines. *Sci. Rep.* 7, 41163. doi:10.1038/srep41163

Elmore, S. (2007). Apoptosis: a review of programmed cell death. *Toxicol. Pathol.* 35, 495–516. doi:10.1080/01926230701320337

Estarabadi, H., Atyabi, S. A., Tavakkoli, S., Noormohammadi, Z., Gholami, M. R., Ghiaseddin, A., et al. (2021). Cold atmospheric plasma induced genotoxicity and cytotoxicity in esophageal cancer cells. *Mol. Biol. Rep.* 48, 1323–1333. doi:10.1007/s11033-021-06178-3

Ferlay, J., Colombet, M., Soerjomataram, I., Parkin, D. M., Pineros, M., Znaor, A., et al. (2021). Cancer statistics for the year 2020: an overview. *Int. J. Cancer* 149, 778–789. doi:10.1002/ijc.33588

Fridman, G., Friedman, G., Gutsol, A., Shekhter, A. B., Vasilets, V. N., Fridman, A., et al. (2008). Applied plasma medicine. *Plasma process. Polym.* 5, 503–533. doi:10.1002/ppap.200700154

Friedl, P., and Wolf, K. (2003). Tumour-cell invasion and migration: diversity and escape mechanisms. *Nat. Rev. Cancer* 3, 362–374. doi:10.1038/nrc1075

Gan, L., Duan, J., Zhang, S., Liu, X., Poorun, D., Liu, X., et al. (2019). Cold atmospheric plasma ameliorates imiquimod-induced psoriasiform dermatitis in mice by mediating antiproliferative effects. *Free Radic. Res.* 53, 269–280. doi:10.1080/10715762.2018.1564920

Gay-Mimbrera, J., Garcia, M. C., Isla-Tejera, B., Rodero-Serrano, A., Garcia-Nieto, A. V., Ruano, J., et al. (2016). Clinical and biological principles of cold atmospheric plasma application in skin cancer. *Adv. Ther.* 33, 894–909. doi:10.1007/s12325-016-0338-1

Gumbel, D., Gelbrich, N., Weiss, M., Napp, M., Daeschlein, G., Sckell, A., et al. (2016). New treatment options for osteosarcoma - inactivation of osteosarcoma cells by cold atmospheric plasma. *Anticancer Res.* 36, 5915–5922. doi:10.21873/anticanres.11178

Haralambiev, L., Wien, L., Gelbrich, N., Lange, J., Bakir, S., Kramer, A., et al. (2020). Cold atmospheric plasma inhibits the growth of osteosarcoma cells by inducing apoptosis, independent of the device used. *Oncol. Lett.* 19, 283–290. doi:10.3892/ol.2019.11115

Ishaq, M., Han, Z. J., Kumar, S., Evans, M. D. M., and Ostrikov, K. (2015). Atmospheric-Pressure plasma- and TRAIL-induced apoptosis in TRAIL-resistant colorectal cancer cells. *Plasma process. Polym.* 12, 574–582. doi:10.1002/ppap.201400207

Kang, S. U., Seo, S. J., Kim, Y. S., Shin, Y. S., Koh, Y. W., Lee, C. M., et al. (2017). Comparative effects of non-thermal atmospheric pressure plasma on migration and invasion in oral squamous cell cancer, by gas type. *Yonsei Med. J.* 58, 272–281. doi:10.3349/ymj.2017.58.2.272

Kim, G. J., Kim, W., Kim, K. T., and Lee, J. K. (2010). DNA damage and mitochondria dysfunction in cell apoptosis induced by nonthermal air plasma. *Appl. Phys. Lett.* 96, 021502. doi:10.1063/1.3292206

Kim, H. J., Barsevick, A., and Tulman, L. (2007). Treatment-related symptom clusters in breast cancer. *Oncol. Nurs. Forum* 34, 192.

Lee, J. H., Om, J. Y., Kim, Y. H., Kim, K. M., Choi, E. H., Kim, K. N., et al. (2016). Selective killing effects of cold atmospheric pressure plasma with NO induced dysfunction of epidermal growth factor receptor in oral squamous cell carcinoma. *Plos One* 11, e0150279. doi:10.1371/journal.pone.0150279

Li, W., Yu, K. N., Bao, L. Z., Shen, J., Cheng, C., Han, W., et al. (2016). Non-thermal plasma inhibits human cervical cancer HeLa cells invasiveness by suppressing the MAPK pathway and decreasing matrix metalloproteinase-9 expression. *Sci. Rep.* 6, 19720. doi:10.1038/srep19720

Liou, G. Y., and Storz, P. (2010). Reactive oxygen species in cancer. *Free Radic. Res.* 44, 479–496. doi:10.3109/10715761003667554

Lv, W., Sheng, X., Chen, T., Xu, Q., and Xie, X. (2008). Jaceosidin induces apoptosis in human ovary cancer cells through mitochondrial pathway. *J. Biomed. Biotechnol.* 2008, 394802. doi:10.1155/2008/394802

Negrin, G., Eiroa, J. L., Morales, M., Triana, J., Quintana, J., Estevez, F., et al. (2010). Naturally occurring asteriscunolide A induces apoptosis and activation of mitogen-activated protein kinase pathway in human tumor cell lines. *Mol. Carcinog.* 49, 488–499. doi:10.1002/mc.20629

Ralph, A. C. L., Calcagno, D. Q., Souza, L. G. D., de Lemos, T. L. G., Montenegro, R. C., Smith, M. D. C., et al. (2016). Biflorin induces cytotoxicity by DNA interaction in genetically different human melanoma cell lines. *Toxicol. Vitro* 34, 237–245. doi:10.1016/j.tiv.2016.04.007

Ratovitski, E. A., Cheng, X. Q., Yan, D. Y., Sherman, J. H., Canady, J., Trink, B., et al. (2014). Anti-cancer therapies of 21st century: novel approach to treat human cancers using cold atmospheric plasma. *Plasma process. Polym.* 11, 1128–1137. doi:10.1002/ppap.201400071

Semmler, M. L., Bekeschus, S., Schafer, M., Bernhardt, T., Fischer, T., Witzke, K., et al. (2020). Molecular mechanisms of the efficacy of cold atmospheric pressure plasma (CAP) in cancer treatment. *Cancers (Basel)* 12, E269. doi:10.3390/cancers12020269

Tinsley, L. J., and Harris, R. A. (2020). A novel computer-controlled maskless fabrication process for pneumatic soft actuators. *Actuators* 9, 136. doi:10.3390/act9040136

Tochhwang, L., Deng, S., Pervaiz, S., and Yap, C. T. (2013). Redox regulation of cancer cell migration and invasion. *Mitochondrion* 13, 246–253. doi:10.1016/j.mito.2012.08.002

Turrini, E., Laurita, R., Stancampiano, A., Catanzaro, E., Calcabrini, C., Maffei, F., et al. (2017). Cold atmospheric plasma induces apoptosis and oxidative stress pathway regulation in T-lymphoblastoid leukemia cells. *Oxid. Med. Cell. Longev.* 2017, 4271065. doi:10.1155/2017/4271065

Volotskova, O., Hawley, T. S., Stepp, M. A., and Keidar, M. (2012). Targeting the cancer cell cycle by cold atmospheric plasma. *Sci. Rep.* 2, 636. doi:10.1038/srep00636

von Woedtke, T., Schmidt, A., Bekeschus, S., Wende, K., and Weltmann, K. D. (2019). Plasma medicine: a field of applied redox Biology. *Vivo* 33, 1011–1026. doi:10.21873/invivo.11570

Walk, R. M., Snyder, J. A., Srinivasan, P., Kirsch, J., Diaz, S. O., Blanco, F. C., et al. (2013). Cold atmospheric plasma for the ablative treatment of neuroblastoma. *J. Pediatr. Surg.* 48, 67–73. doi:10.1016/j.jpedsurg.2012.10.020

Wang, D. C., Zhao, D., Feng, K. C., Zhang, X. H., Liu, D. P., Yang, S. Z., et al. (2011). The cold and atmospheric-pressure air surface barrier discharge plasma for large-area sterilization applications. *Appl. Phys. Lett.* 98, 161501. doi:10.1063/1.3582923

Wang, L. Y., Yang, X. Y., Yang, C. J., Gao, J., Zhao, Y., Cheng, C., et al. (2019). The inhibition effect of cold atmospheric plasma-activated media in cutaneous squamous carcinoma cells. *Future Oncol.* 15, 495–505. doi:10.2217/fon-2018-0419

Wang, M., Holmes, B., Cheng, X. Q., Zhu, W., Keidar, M., Zhang, L. G., et al. (2013). Cold atmospheric plasma for selectively ablating metastatic breast cancer cells. *Plos One* 8, e73741. doi:10.1371/journal.pone.0073741

Wang, Y. H., Xu, X. J., Zhang, L. F., and Li, H. L. (2014). Mimic of manganese superoxide dismutase induces apoptosis in human acute myeloid leukemia cells. *Leuk. Lymphoma* 55, 1166–1175. doi:10.3109/10428194.2013.825904

Wang, Y. H., Yang, X. L., Han, X., Zhang, L. F., and Li, H. L. (2012). Mimic of manganese superoxide dismutase to induce apoptosis of human non-Hodgkin lymphoma Raji cells through mitochondrial pathways. *Int. Immunopharmacol.* 14, 620–628. doi:10.1016/j.intimp.2012.09.019

Xia, J., Zeng, W., Xia, Y., Wang, B., Xu, D., Liu, D., et al. (2019). Cold atmospheric plasma induces apoptosis of melanoma cells via Sestrin2-mediated nitric oxide synthase signaling. *J. Biophot.* 12, e201800046. doi:10.1002/jbio.201800046

Xu, J. H., Liu, D. Y., Niu, H. L., Zhu, G. F., Xu, Y. W., Ye, D. L., et al. (2017). Resveratrol reverses doxorubicin resistance by inhibiting epithelial-mesenchymal transition (EMT) through modulating PTEN/Akt signaling pathway in gastric cancer. *J. Exp. Clin. Cancer Res.* 36, 19. doi:10.1186/s13046-016-0487-8

Yan, D., Wang, Q., Adhikari, M., Malyavko, A., Lin, L., Zolotukhin, D. B., et al. (2020). A physically triggered cell death via transbarrier cold atmospheric plasma cancer treatment. *ACS Appl. Mat. Interfaces* 12, 34548–34563. doi:10.1021/acsami.0c06500

Yan, D. Y., Sherman, J. H., and Keidar, M. (2017). Cold atmospheric plasma, a novel promising anti-cancer treatment modality. *Oncotarget* 8, 15977–15995. doi:10.18632/oncotarget.13304

Yang, X., Yang, C., Wang, L., Cao, Z., Wang, Y., Cheng, C., et al. (2020). Inhibition of basal cell carcinoma cells by cold atmospheric plasmaactivated solution and differential gene expression analysis. *Int. J. Oncol.* 56, 1262–1273. doi:10.3892/ijo.2020.5009

Zhong, S. Y., Dong, Y. Y., Liu, D. X., Xu, D. H., Xiao, S. X., Chen, H. L., et al. (2016). Surface air plasma-induced cell death and cytokine release of human keratinocytes in the context of psoriasis. *Br. J. Dermatol.* 174 542–552. doi:10.1111/bjd.14236

Zhu, W., Lee, S. J., Castro, N. J., Yan, D. Y., Keidar, M., Zhang, L. G., et al. (2016). Synergistic effect of cold atmospheric plasma and drug loaded core-shell nanoparticles on inhibiting breast cancer cell growth. *Sci. Rep.* 6, 21974. doi:10.1038/srep21974